JOURNAL OF MATERIALS SCIENCE 34 (1999) 2773–2779

The photoelectrochemistry of transition metal-ion-doped TiO_2 nanocrystalline electrodes and higher solar cell conversion efficiency based on Zn^{2+}-doped TiO_2 electrode

YANQIN WANG, YANZHONG HAO, HUMIN CHENG*, JIMING MA, BIN XU, WEIHUA LI, SHENGMIN CAI
Department of Chemistry, Peking University, Beijing 100871, People's Republic of China

Metal-ion-doped TiO_2 nanoparticles were prepared with hydrothermal method. The change of photocurrents at different electrode potentials and wavelengths of incident light showed two different characteristics for various transition metal-ion-doped TiO_2 electrodes. In Zn^{2+} and Cd^{2+}-doped TiO_2 electrodes, a characteristic of n-type semiconductor was observed and the incident photon to conversion efficiency (IPCE) were larger than that of pure TiO_2 electrode at the thickness of electrode film of 0.5 μm when the content of doped metal ion was less than 0.5%. The effect of the thickness of films on IPCE was also investigated. The IPCE of pure TiO_2 electrode was strongly dependent on the thickness of films. The change tendency of the IPCE for Zn^{2+}-doped TiO_2 (0.5% Zn^{2+}) electrodes with its thickness was different from that of pure TiO_2. In Fe^{3+}, Co^{2+}, Ni^{2+}, Cr^{3+} and V^{5+}-doped TiO_2 electrodes, a phenomenon of p-n conversion was observed. The difference of photoresponse and the value of photocurrents are dependent on the doping method and concentration of the doped metal ions. The maximum conversion efficiency of $RuL_2(SCN)_2$-sensitized Zn^{2+}-doped TiO_2 solar cell (1.01%) was larger than that of $RuL_2(SCN)_2$-sensitized pure TiO_2 solar cell (0.82%) at the same conditions when 0.5 mol $\cdot$ l^{-1} $(CH_3)_4N \cdot I + 0.05$ mol $\cdot$ l^{-1} I_2 in propylene carbonate solution was used as electrolyte.

1. Introduction

The conversion of solar light into chemical and electric energy has attracted considerable efforts in recent years. Semiconductor materials with nanosized dimension seem to be the most attractive materials. Efficient semiconductor materials for this purpose must possess certain characteristics such as suitable bandgap energy, stability toward photocorrosion and suitable physical characteristics. Of many semiconductor oxides such as Fe_2O_3 [1], ZnO [2, 3], TiO_2 [4], SnO_2 [5], TiO_2 has been shown to be the most suitable material, offering the highest light-conversion efficiency, primarily because of its high stability toward photocorrosion and its relatively favorable bandgap energy.

In the study of solar energy cells, the sensitization of photoanode by narrow bandgap semiconductors such as CdS [6], PbS [7], CdSe [8] or by organic dye [4, 5, 9] was studied extensively. The sensitization of thin films of composite semiconductor [10, 11] was also studied to investigate the mechanism and dynamics of charge injection.

In the field of photocatalysis, the polycrystalline system formed by metal-ion-doped TiO_2 has been the object of several studies [12–17]. In the preparation of metal-ion-doped TiO_2, impregnation [12], coprecipitation [14] and sol-gel method [17] were used, but the hydrothermal method has not been used yet. However, the nanocrystals with good crystallinity can be gained with hydrothermal method.

Although the sensitization of photoanode by narrow bandgap semiconductor or by dye in solar energy cells and the doping of metal ion in TiO_2 photocatalyst have been studied widely, the photoelectrochemical properties of transition metal-ion-doped TiO_2 electrodes were studied scarcely. In this paper, Zn^{2+}, Cd^{2+}, V^{5+}, Cr^{3+}, Fe^{3+}, Co^{2+}, and Ni^{2+}-doped TiO_2 nanoparticles have been prepared with hydrothermal method [18, 19] and the photocurrents of various metal-ion-doped TiO_2 electrodes have also been investigated. Finally, the solar cells conversion efficiency (η) was measured based on tris (2, 2′-bipyridyl-4, 4′-dicarboxylate) ruthenium (II), $RuL_2(SCN)_2$-sensitized Zn^{2+}-doped TiO_2 (0.5% Zn^{2+}) electrodes.

2. Experimental

2.1. The synthesis of metal-ion-doped TiO_2 nanoparticles

The TiO_2 nanoparticles were prepared with hydrothermal method which was reported elsewhere [18, 19]. The pH of reaction media was controlled at pH 1.8.

* Author to whom all correspondence should be addressed.

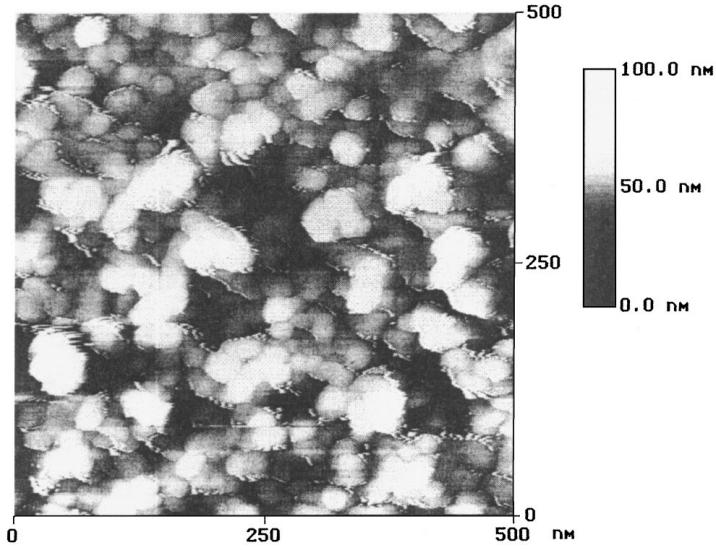

Figure 1 The atom force spectrum (AFM) of TiO_2 electrode.

Metal-ion-doped TiO_2 nanoparticles were prepared according to the same procedure in the presence of added metal salts (except V^{5+} which was obtained by dissolving V_2O_5 in dilute HNO_3) to give an initial doping level of 5% except V^{5+} whose molar content was 0.5%. Metal salts used as precursors for doping ions are listed as follows: $ZnCl_2$, $Cd(NO_3)_2$, $FeCl_3$, $Ni(NO_3)_2$, $Co(NO_3)_2$, and $Cr(NO_3)_3$. In order to study the effect of metal ion content on IPCE, the Zn^{2+}-doped TiO_2 nanoparticles with a doping level of 0.5% were also prepared.

2.2. Characterization of metal-ion-doped TiO_2 nanoparticles

The phase of the reaction products was analyzed by X-ray diffraction (XRD) which uses a CuK_α radiation at 40 kV, 100 mA with a graphite monochromator and scans at 4° min^{-1} (2θ) with a diffractometer (Model Rigaku max-2000). Transmission electron microscope (TEM) (Model JEM-200CX) was used to observe the morphology and particle size of products. Diffuse reflectance spectra (DRS) were recorded by Shimadzu MPS 310 UV-Vis spectrometer equipped with an integration sphere. The element analysis was carried out by ICP.

2.3. The preparation of electrodes

The preparation of electrode was reported elsewhere [19]. In this work, the suspension of TiO_2 or metal-ion-doped TiO_2 with a concentration of 8.0 $g \cdot dm^{-3}$ was dispersed ultrasonically before use. Four drops (ca. 0.2 ml) of the suspension were applied onto a piece of transparent conducting glass (2.0 cm × 1.8 cm, fluorine-doped SnO_2, 50 Ω/sq.) which was heated on a warm plate, then the suspension was spread with a glass rod. The sample was sintered in N_2 at 480 °C for 30 min, cooled to room temperature at once. A layer of porous TiO_2 film formed on the conducting glass. Then another layer of porous film was prepared on the top of the first layer of film. The preparation of multilayer electrode was the same as the above. The final area of electrode was about 0.5 cm^2. The thickness of electrode films was measured with Tencor Alpha-Step Profiler and the morphology of electrode film was observed with atom force microscope (AFM). It can be seen from AFM showed in Fig. 1 that three-dimensional network structure existed with the particle sizes of 20 nm (the unclearness of the surface of some particles was due to the contamination of tip).

The electrodes of different metal ion doped TiO_2 were designated as TM-X where T and M denote TiO_2 and the metal ion, respectively, and X is the content of metal ion. For example, TZn-5 represents Zn^{2+}-doped TiO_2 containing 5% Zn^{2+}.

2.4. Photoelectrochemical measurements of transition metal-ion-doped TiO_2 electrodes

All Photoelectrochemical measurements were carried out by using a standard three-electrode system equipped with a quartz window, a saturated calomel reference electrode (SCE) and a platinum wire counter electrode placed in a separate compartment. 0.1 mol dm^{-3} SCN solution (pH 4.0) was used as electrolyte. A Model 173 potentiostat was used for potentiostatic control and a Type 3036 X-Y Recorder was used for recording the photocurrent. All potentials reported were measured against SCE. The light source was an 200 W xenon lamp and the electrode was illuminated from front-side (the side of metal-ion doped TiO_2 film).

2.5. $RuL_2(SCN)_2$-sensitized TZn-1/2 solar cells

The electrodes were coated with the dye by soaking them overnight (≅12 h) in 5 $mmol \cdot l^{-1}$ of $[RuL_2(SCN)_2]$/absolute ethanol solution at room temperature and then drying them in a warm plate. The films assumed a change of color from orange to red color with the increase of the thickness of films due to adsorption of the dye. To minimize rehydration of

the TiO_2 or TZn-1/2 surface, which causes the dye to desorb, the electrodes were exposed to the dye solution when they were still warm (80–100 °C).

The solar cell conversion efficiency, short-circuit photocurrents and open-circuit photovoltage of $RuL_2(SCN)_2$-sensitized TZn-1/2 electrodes were measured with two-electrode setup. Pt plate coated with a layer of black Pt was squeezed with dye-sensitized electrode using a spring. A solution of propylene carbonate containing 0.5 $mol \cdot l^{-1}$ $(CH_3)_4N \cdot I$ and 0.05 $mol \cdot l^{-1}$ I_2 soaked into toilet paper was used as electrolyte. A 200 W xelon lamp simulating solar spectra was used as light source. The light intensity was 53 mW/cm^2 and measured with an FM-91 photometer. The transmittancy of conducting glass was 57% for visible light.

3. Results and discussion

3.1. XRD analysis

The XRD patterns showed that anatase and brookite coexisted in the samples of metal-ion-doped TiO_2 sintered at 480 °C for 30 min and no separate phase of metal compound appeared except Cr^{3+}-doped TiO_2 in which separate phase of Cr_2O_3 appeared. In our earlier report [19], Fe_2O_3 existed in Fe^{3+}-doped TiO_2 nanoparticles although it can't be detected by XRD. Fig. 2 shows the XRD patterns of pure TiO_2 as well as Cr^{3+}-doped TiO_2. The above results can be explained from the value of the initial pH used for the precipitation of metal ion and the free energy of formation for related oxide. Table I gives the initial pH used for the precipitation of several metal ions.

It can be seen from Table I that the hydrolysis of Fe^{3+} and V^{5+} occurred at pH 1.8, while the formation of Cr_2O_3 phase may be due to that its free energy of formation is lower than that of related hydrate.

TABLE I The initial pH of the precipitation of metal ions [20, 21]

Metal ion	Ni^{2+}	Co^{2+}	V^{5+}	Fe^{3+}	Cr^{3+}	Cd^{2+}	Zn^{2+}
pH	>7	>7	<0	0.76	4.6	6.2	6.7

TABLE II The molar content of metal ions in metal-ion-doped TiO_2

Metal ions	Ni^{2+}	Cd^{2+}	Zn^{2+}	Cr^{3+}	Co^{2+}	Fe^{3+}
Content of ions (%)	0.10	0.1	4.75	4.83	0.18	5.50

3.2. TEM

The morphology and particle sizes (~10 nm) of metal-ion-doped TiO_2 nanoparticles were similar as pure TiO_2 nanoparticles prepared at the same conditions except Fe^{3+}-doped TiO_2 in which small particles (TiO_2) with the particle size of 10 nm and larger particles (α-Fe_2O_3) with the particle size of 50–100 nm coexisted [19].

3.3. The element analysis

The ICP analysis gave the content of metal ions in metal-ion-doped TiO_2 nanoparticles. Table II shows the analytical results which were in agreement with the results of XRD except Zn^{2+}-doped TiO_2 in which the content of Zn^{2+} was 4.75%. In Zn^{2+}-doped TiO_2 nanoparticles, no separate phase of zinc oxide or other zinc compound was detected through XRD.

It can be seen from the results of XRD and element analysis (as well as the data of the initial pH used for the precipitation of metal ions) that Fe^{3+}, Cr^{3+}, V^{5+} and Zn^{2+} ions can hydrolyzed entirely at pH 1.8 although the separate phase of zinc oxide cannot be detected by XRD. It may be attributed to a fact that ZnO was ill crystallizing and adsorbed on the surface of TiO_2 uniformly. For Ni^{2+}, Co^{2+} and Cd^{2+}-doped TiO_2, a small part of metal ions entered into the lattice of TiO_2 or were adsorbed on the surface of TiO_2 and most port of them kept in the solution and eluted through filtration.

3.4. DRS

The DRS showed that the absorption of Zn^{2+}, Ni^{2+} or Co^{2+}-doped TiO_2 was similar as pure TiO_2, the threshold of absorption was nearly unchanged and no obviously enhanced absorption was found in longer wavelength (which may be due to the content of Ni^{2+} or Co^{2+} was very small in these two ions-doped TiO_2 nanoparticles), while the absorption of Cr^{3+}, Fe^{3+}, V^{5+}-doped

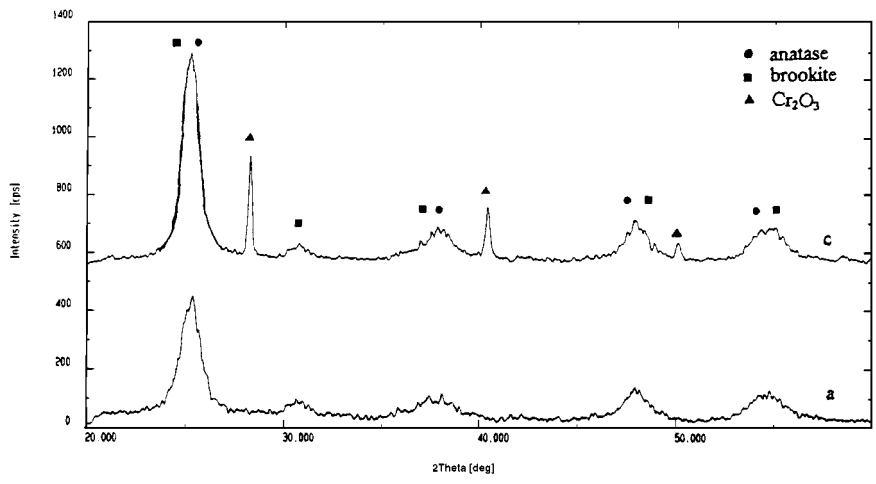

Figure 2 The XRD pattern of pure TiO_2 and Cr^{3+}-doped TiO_2 nanoparticles.

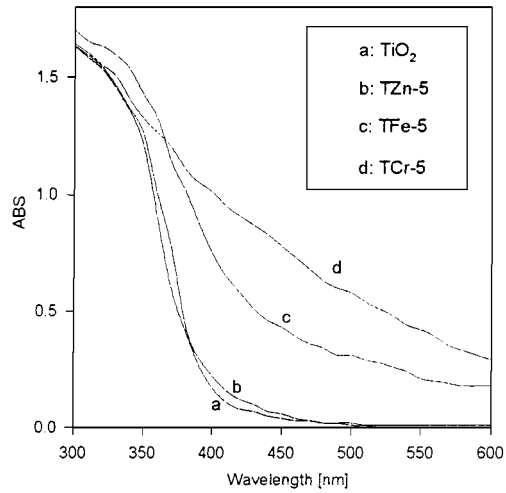

Figure 3 The DRS of four selected samples.

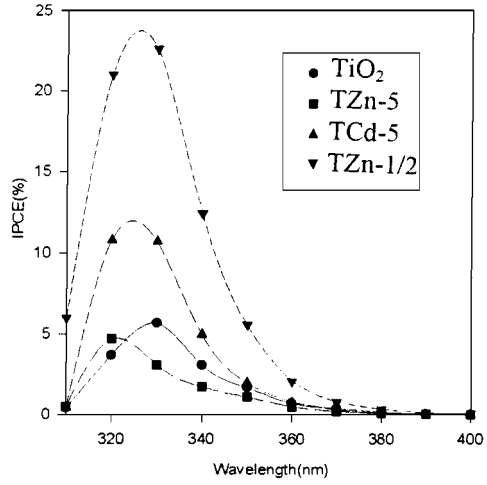

Figure 4 The photocurrent action spectra for metal-ion-doped TiO_2 electrodes.

TiO_2 extended to longer wavelength apparently. Fig. 3 shows the DRS of some representative samples.

3.5. The photoelectrochemical properties of transition metal-ion-doped TiO_2 electrodes

The change of photocurrents with electrode potentials and wavelengths of incident light showed two different characteristics for metal-ion-doped TiO_2 electrodes. For Zn^{2+} and Cd^{2+}-doped TiO_2 electrodes, a characteristic of n-type semiconductor was observed; however, for Fe^{3+}, Co^{2+}, Ni^{2+}, Cr^{3+} and V^{5+}-doped TiO_2 electrodes, a phenomenum of p-n conversion was observed.

3.5.1. The characteristic of n-type semiconductor

Fig. 4 shows the photocurrent action spectra of four electrodes at the electrode potential of +0.3 V when the thickness of electrode film was 0.5 μm. The incident monochromatic photon to current conversion efficiency (IPCE), defined as the number of electrons generated by light in the external circuit divided by the number of

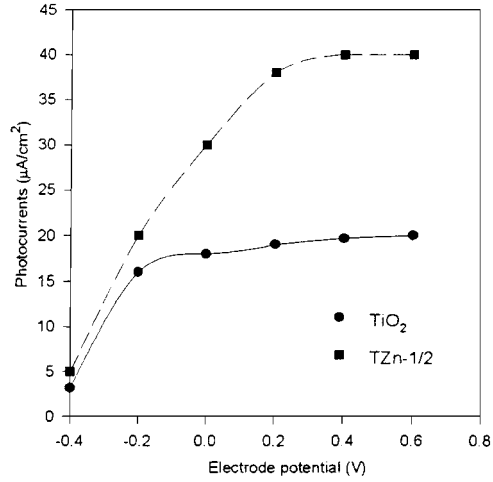

Figure 5 Photocurrent–potential curves for TiO_2 and Zn-1/2 electrodes (Incident light intensity: 8.7 $\mu A/cm^2$).

incident photons, is plotted as a function of excitation wavelength. This was derived from the photocurrents by means of Equation 1 [9]

$$\text{IPCE}\,(\%) = \frac{1.24 \times 10^3 \times i_{sc}(\mu A/cm^2)}{\text{Wavelength}\,(\text{nm}) \times I_{nc}(W/m^2)} \qquad (1)$$

where i_{sc} is photocurrent density, I_{nc} is light intensity.

For comparison with Cd^{2+}-doped TiO_2 (the content of Cd^{2+} was 0.1% by ICP), Zn^{2+}-doped TiO_2 containing 0.5% Zn^{2+} was also prepared and its IPCE was also measured for TZn-1/2 electrode. It can be seen that the IPCE of TZn-1/2 and TCd-5 were larger than that of pure TiO_2, while the IPCE of TZn-5 were the same as that of pure TiO_2 at all wavelength range. Fig. 5 shows the photocurrent-potential curves of TiO_2 and TZn-1/2 at the wavelength of 350 nm which also demonstrates the same tendency. Fig. 5 also shows that the photocurrents were very small at negative potentials, increased rapidly with increasing potential, and then reached saturation at a potential of about +0.2 V for TZn-1/2, −0.2 V for TiO_2 electrode, respectively.

The effect of the thickness of films on IPCE was also studied. The results shown in Fig. 6a and b indicate that the IPCE increased with the thickness of films first and reached maximum at a certain thickness, then reduced with the further increase of the film thickness. Fig. 7 shows the change of IPCE with the thickness of electrode film at the wavelength of 320 nm. The IPCE of pure TiO_2 electrodes demonstrated a different characteristic with that of TZn-1/2 and TCd-5 electrodes as a function of film thickness. The IPCE of pure TiO_2 electrodes increased rapidly from a very small value at a thickness of 0.5 μm to a much large value at a thickness of 0.9 μm, reached a maximum at 1.3 μm, and then reduced slowly at 1.6 μm. However, the IPCE of TZn-1/2 and TCd-5 electrodes increased slowly from a high value at 0.5 μm to a much larger value at 0.9 μm and also reached a maximum at 1.3 μm, then reduced rapidly at 1.6 μm. It also shows that the TZn-1/2 and TCd-5 electrodes had much larger IPCE than that of pure TiO_2 at the thickness of 0.5 μm. At the thickness of 0.9 μm, TZn-1/2 electrode had a little larger value

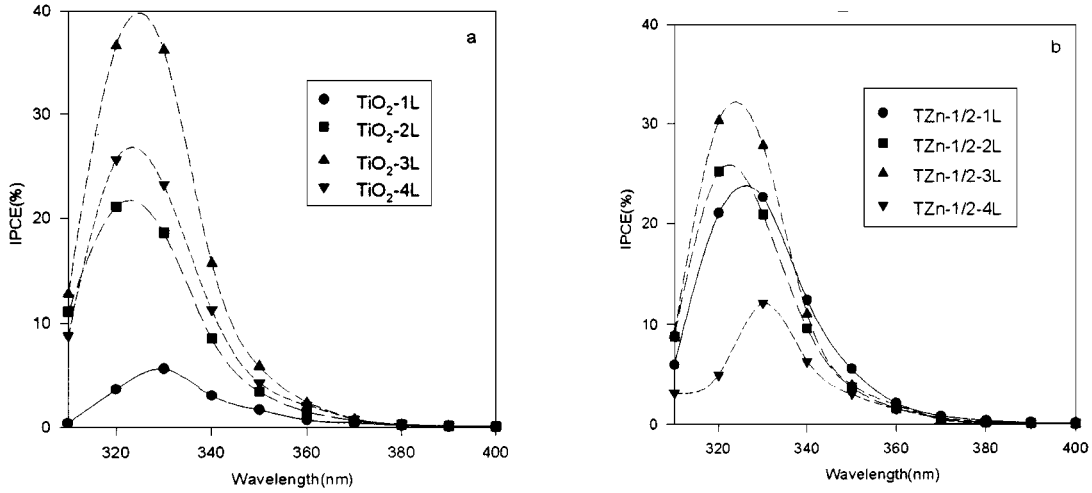

Figure 6 The photocurrent action spectra at different thickness for TiO_2 and TZn-1/2 electrodes (1L-0.5, 2L-0.9, 3L-1.3 and 4L-1.6 μm).

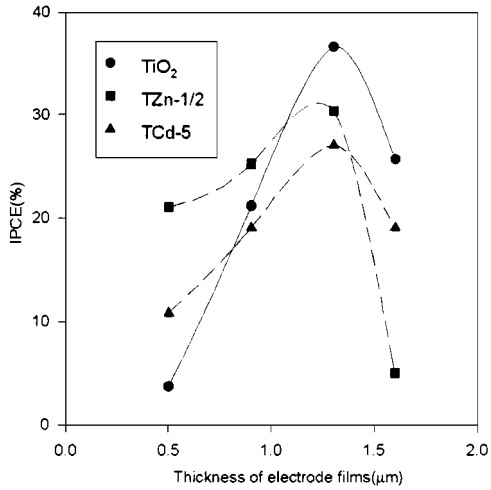

Figure 7 The IPCE versus the layers of electrode film (Illumination at 320 nm with the light intensity of 5.5 μA/cm^2).

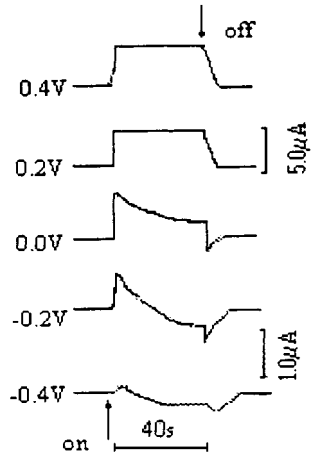

Figure 8 The transient photocurrent of Co^{2+}-doped TiO_2 electrode at different potentials (Illumination at 350 nm with the light intensity of 38.7 μW/cm^2).

but TCd-5 had a little smaller value than that of pure TiO_2. At the thickness of 1.3 and 1.6 μm, the order of the photocurrent magnitude was inversed, i.e., the IPCE of pure TiO_2 electrodes was larger than that of TZn-1/2 and TCd-5 electrodes.

3.5.2. The characteristic of p-n photoresponse conversion

The phenomena of p-n conversion were observed extensively in Fe^{3+}, Co^{2+}, Ni^{2+}, Cr^{3+} and V^{5+}-doped TiO_2 electrodes when monochromatic light of the wavelength of 350 nm was used as incident light. It can be seen from measuring the photocurrents at different electrode potentials that cathodic photocurrent (p-type photoresponse) appeared at negative potentials, and then converted to anodic photocurrents (n-type photoresponse) at positive potentials except Fe^{3+}-doped TiO_2 in which the cathodic photocurrent sustained at potential of +0.2 V [19]. As a typical case, Fig. 8 shows the transient photocurrents at different potentials for Co^{2+}-doped TiO_2 electrode. When the electrode potential was less than +0.2 V, an anodic photocurrent generated rapidly at the beginning of illumination, decayed to a steady photocurrent with the time of illumination, then a downward peak of cathodic photocurrent appeared when the light was chopped off. The downward peak generated from the reaction of electrons in the conduction band of TiO_2 with the acceptor such as O_2 or $(SCN)_2$ in solution because no band bending in TiO_2 nanoporous film [22]. In more positive potentials, there was no decay of the photocurrent and no downward peak because of the fast transfer of electrons through out-circuit.

In order to investigate the real existence of p-n junction the transient photocurrents of Fe^{3+}, Co^{2+}, Ni^{2+}, Cr^{3+} and V^{5+}-doped TiO_2 nanoporous electrodes were measured at electrode potential of +0.3 V as a function of the wavelength of incident light. The similar phenomena of p-n conversion appeared and the result for Co^{2+}-doped TiO_2 was shown in Fig. 9. It can be seen from Fig. 9 that the cathodic photocurrent generated at the beginning of illumination, then converted to a steady anodic photocurrent at a wavelength of 320 nm, followed by a steady anodic photocurrent at the range of 330–400 nm, and finally a cathodic photocurrent appeared again.

The actual doping concentration of transition metal ions in TiO_2 is related to the ionic radii. Table III shows the ionic radii for a coordination number of 6. It can be seen from Table III that Fe^{3+}, Ni^{2+}, Cr^{3+} and V^{5+}

TABLE III The ionic radii for a coordination number of 6 [23]

Ion	Fe^{3+}	Co^{2+}	Ni^{2+}	Cr^{3+}	V^{5+}	Zn^{2+}	Cd^{2+}	Ti^{4+}
Ionic radii (Å)	0.645	0.745	0.69	0.615	0.54	0.74	0.95	0.605

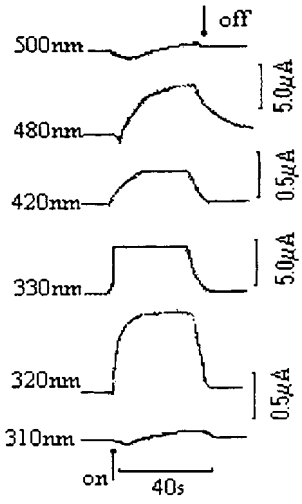

Figure 9 The transient photocurrent of Co^{2+}-doped TiO_2 electrode at different wavelengths (electrode potential +0.3 V).

may enter into the lattice of TiO_2 easier, while Co^{2+}, Zn^{2+} and Cd^{2+} were difficult to enter into the lattice of TiO_2. The concentration of metal ions entered into the lattice of TiO_2 were very small. In transition metal-ion-doped TiO_2 nanoparticles, metal ions entered into the lattice of TiO_2 to form solid solution. The existence of p-n junction can be explained from the formation of the microzone of p-type by substituting lowervalent metal ions for Ti^{4+} in TiO_2 [24]. The formation of microzone of p-type in V^{5+}-doped TiO_2 may be related to the change of V^{5+} valance. While for Zn^{2+} and Cd^{2+}-doped TiO_2, the phenomena of p-n coexistence were not been observed, which may be due to that Zn^{2+} and Cd^{2+} entered into the interstitial of the lattice of TiO_2 and increased the electrons in conduction band [24].

In a recent report [25], chemically modified Ni/TiO_2 nanocomposite films also showed the characteristic of p-n conversion. The bandgap energy of the solid solution is smaller than that of pure TiO_2 (in accordance with DRS) and the cathodic photocurrent (p-type photoresponse) competed and offsetted with anodic photocurrent (n-type photoresponse). At negative potentials, the cathodic photocurrent predominated in determining the sign of the photocurrent, while the anodic photocurrent predominated in determining the sign of the photocurrent at positive potentials. The photocurrents were much smaller than that of pure TiO_2 because of the mutual offset of anodic and cathodic photocurrents at positive potential.

For Zn^{2+} and Cd^{2+}-doped TiO_2 nanoparticles, solid solution was also formed with a very low content of metal ions, so separate phase of ZnO was formed when the content of Zn^{2+} was 5% although ZnO can not be detected by XRD, it may adsorbed on the surface of TiO_2 as ill crystals. The doping of Zn^{2+} and Cd^{2+} ions in TiO_2 formed the permanent electric field, as the content of doping metal ion increases, the space charge layer becomes thinner which favors the separation of photogenerated electron-hole pairs, but if the concentration of doping ion is too high, the space charge layer is very thin, the penetration depth of light is larger than the space charge layer and the electron-hole pairs photogenerated in the inner of TiO_2 recombines easier before it reaches the out-circuit. Another factor reduced the photocurrents may be due to the formation of separate phase when the concentration of doping ion is high. So there is a optimal doping concentration which makes the space charge layer be equal to the penetration depth of light.

The change of photocurrents with the thickness of films may be related to the absorption to light, the depth of light penetration, the separation of carriers and the resistance of electrons traversing the electrode films.

3.6. $RuL_2(SCN)_2$-sensitized Zn^{2+}-doped TiO_2 (0.5% Zn^{2+}) solar cells

Table IV shows the shirt-circuit photocurrents (i_{sc}), open-circuit photovoltage (V_{oc}), fill factor (ff) and solar cell conversion efficiency (η) of Zn^{2+}-doped TiO_2 electrode at different thickness of films.

It can be seen that the fill factor (ff) changed only a little and open-circuit photovoltage (V_{oc}) increased from 0.56 V at the thickness of 0.5 μm to a larger value of 0.68 V at the range of 0.9–2.5 μm, and then reduced to 0.66 V at the thickness of 3.1 μm. Meanwhile the short-circuit currents and solar cells conversion efficiency increased gradually with the thickness of electrode films, reached maximum at the thickness of 2.0 μm, and then decreased with the further increase of the thickness of films.

The maximum conversion efficiency (0.82%) for $RuL_2(SCN)_2$-sensitized TiO_2 without dopant was also obtained at the thickness of 2.0 μm. The open-circuit voltage was 0.617 V, short-circuit voltage was 0.92 mA/cm^2 and fill factor was 0.42, respectively. Fig. 10 shows the i–V characteristic curves for $RuL_2(SCN)_2$-sensitized TiO_2 and TZn-1/2 solar cells with the maximum conversion efficiency.

From the above results, we can see that the maximum conversion efficiency and open-circuit voltage of Zn^{2+}-doped TiO_2 (containing 0.5% Zn^{2+}) were larger than that of TiO_2 solar cell at the same conditions. In our

TABLE IV Parameters of $RuL_2(SCN)_2$-sensitized TZn-1/2 solar cells with the thickness of films

Thickness parameters	0.5 μm	0.9 μm	1.3 μm	1.6 μm	2.0 μm	2.5 μm	3.1 μm
i_{sc}(mA/cm^2)	0.066	0.240	0.396	0.579	1.00	0.700	0.506
V_{oc}(V)	0.560	0.670	0.680	0.680	0.680	0.670	0.660
ff	0.47	0.46	0.43	0.45	0.45	0.41	0.46
η(%)	0.053	0.24	0.38	0.58	1.21	0.64	0.51

Intensity of incident light: 53 mW/cm^2
Transmittancy of conducting glass: 57%
ff = maximum output power/(short-circuit current × open-circuit voltage)

$$\eta\,(\%) = \frac{\text{short-circuit current (mA/cm}^2) \times \text{open-circuit voltage(V)} \times \text{ff}}{\text{light intensity (mW/cm}^2) \times \text{transmissive coefficient}}$$

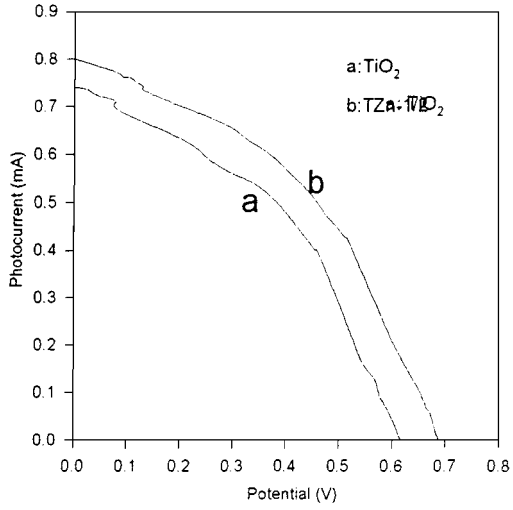

Figure 10 The *i-V* characteristic curves for $RuL_2(SCN)_2$-sensitized TiO_2 and TZn-1/2 solar cells. 0.5M $(CH_3)_4N \cdot I + 0.05M\ I_2$ propylene carbonate solution as electrolyte. The area of electrode was 0.8 cm^2.

experimental conditions, the conversion efficiency of solar cells was small (1.2%) comparing with Gratzel's work [4, 9], which may be due to the poor electrolyte (in latter, $0.5\,mol \cdot l^{-1}$ LiI + $0.05\,mol \cdot l^{-1}\ I_2$ in ethylene carbonate + propylene carbonate solution was used as electrolyte and Li^+ ion plays a role in increasing the short-circuit photocurrent), high square ohm of conducting glass (in latter, the square ohm was 8 Ω), the imperfect design of solar cells and other factors. The optimum conditions to improve the conversion efficiency will be investigated in our next work. The other results for $RuL_2(SCN)_2$-sensitized metal-ion-doped TiO_2 solar cells will be reported recently.

Acknowledgement

Support from the National Natural and Science Foundation of China (project number 29673003) and Doctoral Program Foundation of Higher Education is gratefully acknowledged.

References

1. U. BJORKSTEN, J. MOSER and M. GRÄTZEL, *Chem. Mater.* **6** (1994) 858–863.
2. S. HOTCHANDANI and P. V. KAMAT, *J. Electrochem. Soc.* **139** (1992) 1630.
3. K. RENSMO, K. KEIS, H. LINDSTROM *et al.*, *J. Phys. Chem. B* **101** (1997) 2598–2601.
4. B. O. REGAN and M. GRÄTZEL, *Nature* **353** (1991) 737–739.
5. I. BEDJA and P. V. KAMAT, *J. Phys. Chem.* **99** (1995) 9187.
6. R. VOGEL, K. POUL and H. WELLER, *Chem. Phys. Lett.* **174** (1990) 241.
7. R. VOGEL, K. POUL and H. WELLER, *J. Phys. Chem.* **98** (1994) 3183.
8. DILIU and P. V. KAMAT, *J. Electroanal. Chem.* **347** (1993) 451.
9. M. K. NAZEERUDDIN, A. KAY and M. GRÄTZEL, *J. Amer. Chem. Soc.* **115** (1993) 6832.
10. S. HOTCHANDANI and P. V. KAMAT, *Chem. Phys. Lett.* **191** (1992) 320.
11. C. NASR, S. HOTCHANDANI and P. V. KAMAT, *J. Phys. Chem. B* **101** (1997) 7480.
12. M. I. LITTER and J. A. NAVIO, *J. Photochem. Photobiol. A Chem.* **98** (1994) 183.
13. M. I. LITTER and J. A. NAVIO, *J. Mol. Catal.* **106** (1996) 267.
14. L. PALAMISONO, V. AUGUGLIAO, A. SCLAFANI *et al.*, *J. Phys. Chem.* **92** (1983) 6710–6713.
15. J. SORIA, J. C. CONESA, V. AUGUGLIARO, *et al.*, *J. Phys. Chem.* **95** (1991) 274–282.
16. E. K. KARAKITSOU and X. E. VERYKIOS, *J. Phys. Chem.* **97** (1993) 1184–1189.
17. WONGYONG CHOI, A. TERMIN and M. R. HOFFERMANN, *J. Phys. Chem.* **98** (1994) 13669–13679.
18. HUMIN CHENG, JIMIN MA *et al.*, *Chem. Mater.* **7** (1995) 663–671.
19. YANQIN WANG, HUMINCHENG and YANZHONG HAO *et al.*, *J. Mater. Sci.*, accepted.
20. "Inorganic Chemistry," People's Education, Shanghai (1978).
21. G. SVEHLA, "Vogel's Textbook of Macro and Semimacro Qualitative Inorganic Analysis," 5th ed. (1978).
22. A. HAGFELDT and M. GRÄTZEL, *Chem. Rev.* **95** (1995) 49–68.
23. R. D. SHANNON, *Acta Cryst.* **A32** (1976) 751.
24. MIEZENG SU, "Introduction of solid chemistry," Peking University (1987).
25. N. DE TACCONI, J. CARMONA and K. RAJESHWAR, *J. Phys. Chem. B* **101** (1997) 10151–10154.

Received 27 October
and accepted 18 November 1998